

HEAT TRANSFER IN WATER BASED NANOFLUIDS (TiO₂-H₂O, Al₂O₃-H₂O and Cu-H₂O) OVER A STRETCHING CYLINDER

M. M. Rahman*, A. Aziz^o

*Department of Mathematics and Statistics, College of Science, Sultan Qaboos University, P.O. Box 36, P.C. 123 Al-Khod, Muscat, Sultanate of Oman

^oDepartment of Mechanical Engineering, School of Engineering and Applied Science, Gonzaga University, Spokane, WA 99258, USA

ABSTRACT

Two-dimensional steady natural convection heat transfer to water based nanofluids (TiO₂-water, Al₂O₃-water, and Cu-water) flowing over a stretching cylinder has been investigated numerically. Using the similarity transformations, the continuity, momentum, and energy equations are reduced to a set of nonlinear, ordinary differential equations. These equations are solved numerically using MATLAB. Because of the algebraic decay of the similarity functions, numerical integration is performed using a compressed coordinate. The axial velocity is the result of forced convection due to stretching, and natural convection induced by the heated cylinder. The results show that the flow velocity with a nanofluid is smaller compared with the velocity of the base fluid for the same stretching and heating conditions, which is basically caused by the increase of viscosity and density. The presence of nanoparticles reduces the thickness of the hydrodynamic boundary layer and enhances the heat transfer rate. The location of the zero shear stress on the surface of the cylinder occurs at shorter and shorter distances (along the cylinder) as the solid volume fraction of nanoparticles increases.

Keywords: Nanofluid, heat transfer, stretching cylinder, convection, similarity solution

1. INTRODUCTION

A base fluid containing suspension of ultra fine metallic or non-metallic nanometer-sized (usually less than 100 nm) solid particles or fibers was first given the name nanofluid by Choi [1]. Compared with conventional base fluids such as water, engine oil, ethylene glycol, toluene, etc., the thermal conductivities of nanofluids containing either metallic nanoparticles (e.g. Cu, Al, Fe, Hg, and Ti) or non-metallic nanoparticles (e.g. Al₂O₃, CuO, SiO₂, TiO₂) are an order of magnitude higher even when the concentration of nanoparticles is small. Besides offering higher thermal conductivities, today's nanofluids offer other advantages such as minimal clogging of flow passage, long term stability, and homogeneity compared with fluids containing micro- or milli-sized particles (Masuda et al. [2], Lee et al. [3], Xuan and Li [4], and Xuan and Roetzel [5]). Because of enhanced heat transfer characteristics, nanofluids can be effectively utilized in several industrial applications such for transportation, chemical production, production of microelectronics, automobiles, power generation in a power plant, advanced nuclear systems (Buongiorno [6]), and nano-drug delivery (Kleinstreuer et al. [7]).

Convective heat transfer in nanofluids has become a topic of major contemporary interest in science and technology. During the past decade, considerable research has been conducted to study the heat transfer enhancement achievable with nanofluids (see, Eastman et al. [8], Murshed et al. [9]). Many researchers (e.g., Khanafer et al. [10], Maiga et al. [11], Jou and Tzeng [12], Hwang et al. [13], Tiwari and Das [14], Oztop and Abu-Nada [15], Abu-Nada and Oztop [16], Muthamilselvan et al. [17], Kuznetsov and Nield [18],

Bachok et al. [19], Khan and Aziz [20], Aziz and Khan [21], Rahman et al. [22], Rahman and Eltayeb [23]) have reported results on convective heat transfer in nanofluids in different geometries and under different flow conditions. Excellent reviews on convection in nanofluids have been published by Kakac and Pramuanjaroenkij [24], Das et al. [25], Trisaksri and Wongwises [26], Wang and Mujumdar [27-28].

The flow induced by a stretching surface is important in engineering studies because the fluid entrained during the process affects the thermal resistance and hence the cooling of the final product. Experiments have indicated that the velocity of a stretching surface is approximately proportional to the distance from the orifice. Crane [29] first studied the flow caused by an elastic sheet whose velocity varies linearly with the distance from a fixed point on the sheet. Since then many investigators (see Wang [30], Andersson et al. [31]; Elbashbeshy [32]; Rahman and Lawatia [33]; Rahman [34] and the references there in) have studied and reported results on flow and heat transfer characteristics of stretching sheets. Brady and Acrivos [35] considered the flow inside a stretching tube, while Wang [36] studied the same flow outside a stretching cylinder. The forced convection problem on a stretching cylinder, including suction/blowing, was studied by Ishak et al [37]. Recently, Wang [38] has studied natural convection on a vertical stretching cylinder and obtained similarity type solutions analyzing the asymptotic behavior of the solutions for large Reynolds number.

The subject of nanofluid flows is relatively new and a number of models (e.g. Buongiorno [6], Tiwari and Das [14]) have been advocated to characterize the convective process in nanofluids. At this nascent stage of development, the proposed models are based on several simplifying

assumptions which have resulted in some controversies about the validity of different models. Khan and Pop [39] studied forced convective boundary layer flow of a nanofluid past a stretching surface, while Hamad and Pop [40] studied the boundary layer flow near a stagnation-point on a heated permeable stretching surface in a porous medium saturated with a nanofluid with heat generation and absorption. Following the work of Tiwari and Das [14], Hamad and Pop [40] considered a single-phase model in which both the base fluid and the solid particles are in thermal equilibrium with each other and have the same local velocity. The advantage of Tiwari and Das model is the availability of the physical parameter values. Following the approach of Tiwari and Das [14], and Hamad and Pop [40], Sebdani et al. [41] investigated the effect of nanofluid variable properties on mixed convection in a square cavity. Kuznetsov and Nield [42] studied double-diffusive natural convective boundary-layer flow of a nanofluid past a vertical plate while Nield and Kuznetsov [43] studied the Cheng–Minkowycz problem for the double-diffusive natural convective boundary layer flow in a porous medium saturated by a nanofluid. Travis et al. [44] argued that because nanofluid is a suspension it cannot be modeled as a Newtonian fluid. This point was further scrutinized by Straughan [45].

The objective of the present study is to apply the model proposed by Wang [38] to investigate natural convection in water based nanofluids over a stretching cylinder which is applicable in the extrusion of seamless tubes. By using proper transformations, the governing equations are reduced to similarity equations and solved numerically. These solutions provide a basic insight into the effect of the various parameters on the heat transfer characteristics of the flow with only modest computational effort. Graphs and tables are presented to illustrate and discuss important hydrodynamic and thermal features of the flow. The accompanying discussion provides physical interpretations of the results.

The organization of the remainder of the paper is as follows. In Section 2 we describe the mathematical model and discuss the non-dimensionalization of the governing equations. The algebraic decay of the solutions is discussed in Section 3. Section 4 discusses briefly the solution method. The results are summarized and discussed in Section 5. Section 6 highlights the important conclusions derived from the present study.

2. FORMULATION OF THE PROBLEM

2.1 Flow analysis

We consider a steady two-dimensional laminar flow of a viscous, incompressible water based nanofluid of density ρ_{nf} and temperature T_∞ moving over the heated surface of a vertical cylinder of radius a . The surface of the cylinder is stretched with a linear velocity $2kz$, where k is a constant and z is the axial coordinate along the flow direction. Let (u, w) be the velocity components in the (r, z) directions respectively. The flow configurations and the coordinate system are shown in Fig. 1.

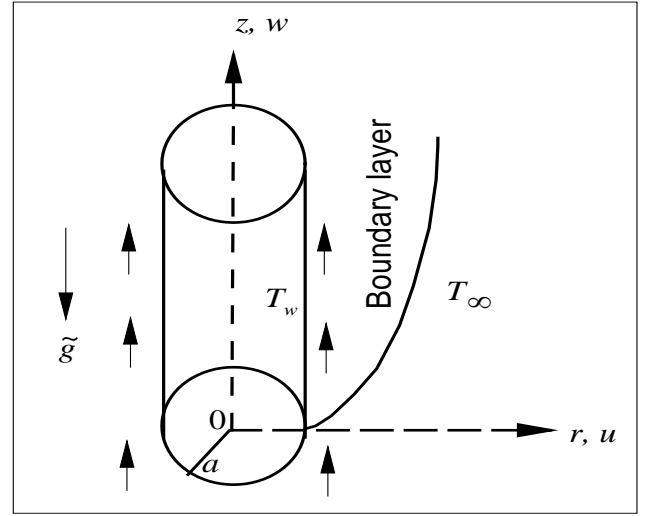


Figure 1 Flow configurations and coordinate system.

We consider the nanofluid as a two-component mixture (i.e. base fluid plus nanoparticles) with the assumptions of incompressible flow, no chemical reactions, dilute mixture, and nanoparticles of uniform shape and size. We further assume that the temperature changes resulting from viscous dissipation are negligible, and that the nanoparticles and the base fluid are locally in thermal equilibrium and flow at the same velocity. The thermophysical properties of the nanofluid are considered to be constant except for the density variation in the buoyancy force (Boussinesq approximation). Under the boundary layer approximations, the axisymmetric continuity, momentum and energy equations (Rahman et al. [22], Wang [38]) may be written as

$$\frac{\partial u}{\partial r} + \frac{u}{r} + \frac{\partial w}{\partial z} = 0, \quad (1)$$

$$u \frac{\partial w}{\partial r} + w \frac{\partial w}{\partial z} = \frac{\mu_{nf}}{\rho_{nf}} \nabla^2 w + \frac{\tilde{g}}{\rho_{nf}} \left[(1-\phi)\rho_{bf}\beta_{bf} + \phi\rho_{sp}\beta_{sp} \right] (T - T_\infty), \quad (2)$$

$$u \frac{\partial T}{\partial r} + w \frac{\partial T}{\partial z} = \alpha_{nf} \nabla^2 T, \quad (3)$$

where T is the temperature of the nanofluid in the boundary layer, \tilde{g} is the acceleration due to gravity, ∇^2 is the Laplace operator defined by

$$\nabla^2 = \frac{\partial^2}{\partial r^2} + \frac{1}{r} \frac{\partial}{\partial r} + \frac{\partial^2}{\partial z^2}. \quad (4)$$

The effective dynamic viscosity (μ_{nf}), density (ρ_{nf}), coefficient of thermal expansion (β_{nf}), thermal diffusivity (α_{nf}), and the heat capacitance (ρc_p)_{nf} of the nanofluid are given as

$$\mu_{nf} = \frac{\mu_{bf}}{(1-\phi)^{2.5}} \quad (\text{Brinkman [46]}), \quad (6)$$

$$\rho_{nf} = (1-\phi)\rho_{bf} + \phi\rho_{sp} \quad (\text{Xuan and Li [47]}), \quad (7)$$

$$(\rho\beta)_{nf} = (1-\phi)\rho_{bf}\beta_{bf} + \phi\rho_{sp}\beta_{sp} \text{ (Mansour and Ahmed [48])}, \quad (8)$$

$$\alpha_{nf} = \kappa_{nf} / (\rho c_p)_{nf}, \quad (9)$$

$$(\rho c_p)_{nf} = (1-\phi)(\rho c_p)_{bf} + \phi(\rho c_p)_{sp} \text{ (Xuan and Li [47])}, \quad (10)$$

where ϕ is the nanoparticle volume fraction. The effective thermal conductivity of the nanofluid can be determined by Maxwell-Garnett's self-consistent approximation model

$$\frac{\kappa_{nf}}{\kappa_{bf}} = \frac{\kappa_{sp} + 2\kappa_{bf} - 2\phi(\kappa_{bf} - \kappa_{sp})}{\kappa_{sp} + 2\kappa_{bf} + \phi(\kappa_{bf} - \kappa_{sp})} \text{ (Hamilton and Crossner [49])}. \quad (11)$$

Equation (11) applies only to spherical nanoparticles but has been found to be satisfactory for studying convective heat transfer in nanofluids (Oztop and Abu-Nada [15]).

The physical quantities μ_{bf} , ρ_{bf} , κ_{bf} , β_{bf} , and $(c_p)_{bf}$, respectively represent the dynamic viscosity, density, thermal conductivity, coefficient of thermal expansion of the base fluid, and specific heat of the base fluid at constant pressure while μ_{sp} , ρ_{sp} , κ_{sp} , β_{sp} , and $(c_p)_{sp}$, respectively represent the same for the solid nanoparticle. The thermo-physical properties of the solid nanoparticles and the nanofluid volume fraction are given in Tables 1 and 2 (Khanafar et al. [10]; Oztop and Abu-Nada [15]; Ho et al. [50]; Das and Ohal [51]).

Table 1 Thermophysical properties of fluid and nanoparticles (Oztop and Abu-Nada [16]).

Physical properties	Fluid phase (H ₂ O)	TiO ₂	Al ₂ O ₃	Cu
C_p (J / kg K)	4179	686.2	765	385
ρ (kg / m ³)	997.1	4250	3970	8933
κ (W / mK)	0.613	8.9538	40	400
$\beta \times 10^{-5}$ (1 / K)	21	0.9	0.63	1.67

Table 2 Effective thermal conductivity (κ_{nf}) of the various water-based nanofluids for different volume concentrations.

ϕ	TiO ₂ - H ₂ O	Al ₂ O ₃ - H ₂ O	Cu- H ₂ O
0.02	0.6436	0.6488	0.6504
0.05	0.6915	0.7053	0.7093
0.01	0.7771	0.8073	0.8163

2.2 Boundary conditions

The applicable boundary conditions for the present model are

$$(i) \text{ on the surface of the cylinder } (r = a):$$

$$u = 0, \quad w = 2kz, \text{ (no-slip and impermeable surface)} \quad (13a)$$

$$T = T_w, \text{ (uniformly heated surface)} \quad (13b)$$

(ii) matching with the quiescent free stream ($r \rightarrow \infty$):

$$w = 0, \quad (13c)$$

$$T = T_\infty, \quad (13d)$$

where the subscript ∞ refers to the edge of the boundary layer.

2.3 Dimensionless variables

We introduce the following dimensionless variables (see Wang [38]):

$$\zeta = \left(\frac{r}{a}\right)^2, \quad (14a)$$

$$u = -ka \frac{f(\zeta)}{\sqrt{\zeta}}, \quad (14b)$$

$$w = 2kzf'(\zeta) + \Lambda g(\zeta), \quad (14c)$$

$$\Lambda = \frac{\tilde{g}\beta_{bf}(T_w - T_\infty)}{2k}, \quad (14d)$$

$$h(\zeta) = \frac{T - T_\infty}{T_w - T_\infty}. \quad (14e)$$

Note that axial velocity w is given by the sum of two terms involving two similarity functions, namely, f' due to forced convection by stretching and g due to buoyancy induced natural convection.

2.3.1 Dimensionless governing equations

After substituting Eqs. (6)-(11) & Eq. (14) into Eqs. (2)-(3) and performing some algebraic manipulation, we obtain the following coupled ordinary differential equations:

$$\zeta f''' + f'' + A \text{Re} [ff'' - f'^2] = 0, \quad (15)$$

$$\zeta g'' + g' + A \text{Re} [fg' - gf'] + B \text{Re} h = 0, \quad (16)$$

$$\zeta h'' + h' + C D \text{Re} Pr fh' = 0, \quad (17)$$

where the constants A , B , C and D are defined by

$$A = (1-\phi)^{2.5} \left[1 - \phi + \phi \left(\frac{\rho_{sp}}{\rho_{bf}} \right) \right], \quad (18)$$

$$B = (1-\phi)^{2.5} \left[1 - \phi + \phi \left(\frac{\rho_{sp}}{\rho_{bf}} \right) \left(\frac{\beta_{sp}}{\beta_{bf}} \right) \right], \quad (19)$$

$$C = \left[1 - \phi + \phi \left(\frac{\rho_{sp}}{\rho_{bf}} \right) \left(\frac{(c_p)_{sp}}{(c_p)_{bf}} \right) \right], \quad (20)$$

$$D = \frac{\kappa_{sp} + 2\kappa_{bf} + \phi(\kappa_{bf} - \kappa_{sp})}{\kappa_{sp} + 2\kappa_{bf} - 2\phi(\kappa_{bf} - \kappa_{sp})}. \quad (21)$$

The dimensionless parameters appeared in Eqs. (15)-(17) are defined as follows:

$\text{Re} = ka^2 / 2\nu_{bf}$ is the Reynolds number corresponding to the base fluid, $Pr = \nu_{bf} / \alpha_{bf}$ is the Prandtl number for the base fluid, $\nu_{bf} = \mu_{bf} / \rho_{bf}$ is the kinematic viscosity of the base fluid.

2.3.2 Dimensionless boundary conditions

The corresponding boundary conditions (13) become

$$f(1) = 0, \quad f'(1) = 1, \quad f'(\infty) = 0, \quad (22a)$$

$$g(1) = 0, g(\infty) = 0, \quad (22b)$$

$$h(1) = 1, h(\infty) = 0. \quad (22c)$$

It may be noted that for $\phi = 0$ i.e. for base fluid the value of the constants A , B , C and D become 1. Therefore, the Eqs. (15)-(17) exactly coincide with the Eqs. (13)-(15) of Wang [38] whereas the boundary conditions for both the models remain the same. Thus, the model of Wang [38] is a special case of the current model when $\phi = 0$.

2.4 Parameters of engineering interest

Skin-friction coefficient

The shear stress on the surface of the cylinder is defined by

$$\tau = \mu_{nf} w_r \Big|_{r=a} = \frac{\mu_{bf}}{(1-\phi)^{2.5}} \left[\frac{4kz}{a} f''(1) + \frac{2\Lambda}{a} g'(1) \right] \quad (23)$$

The skin friction coefficient (rate of shear stress) is defined by

$$\begin{aligned} C_f &= \frac{2\tau}{\rho_{bf} (ka)^2} \\ &= \frac{2\nu_{bf}}{(ka)^2 (1-\phi)^{2.5}} \left[\frac{4kz}{a} f''(1) + \frac{2\Lambda}{a} g'(1) \right] \\ &= \frac{1}{(1-\phi)^{2.5}} \left[\frac{4\xi}{\text{Re}} f''(1) + \frac{\gamma}{4\text{Re}} g'(1) \right], \end{aligned} \quad (24)$$

where $\xi = z/a$ is the nondimensional axial distance, $\gamma = Gr_{bf} / \text{Re}_{bf}^2$ is the Richardson parameter, and $Gr_{bf} = \tilde{g} \beta_{bf} (T_w - T_\infty) a^3 / \nu_{bf}^2$ is the Grashof number.

It is to be noted that the rate of shear stress depends on the axial distance ξ . Thus, the location for zero shear stress is at

$$\xi = -\frac{\gamma}{16} \frac{g'(1)}{f''(1)}. \quad (25)$$

Nusselt number

The Nusselt number (rate of heat transfer) is defined

$$\text{as } Nu = \frac{aq_w}{\kappa_{bf} (T_w - T_\infty)}, \quad (26)$$

where the surface heat flux is defined by,

$$q_w = -\kappa_{nf} T_r \Big|_{r=a} = -\kappa_{nf} \frac{(T_w - T_\infty)}{a} 2h'(1). \quad (27)$$

Using Eq. (27), the Nusselt number i.e., Eq. (26) can be written as

$$\begin{aligned} Nu &= -(\kappa_{nf} / \kappa_{bf}) 2h'(1) \\ &= -\left[\frac{\kappa_{sp} + 2\kappa_{bf} - 2\phi(\kappa_{bf} - \kappa_{sp})}{\kappa_{sp} + 2\kappa_{bf} + \phi(\kappa_{bf} - \kappa_{sp})} \right] 2h'(1) \\ &= -(2/D)h'(1). \end{aligned} \quad (28)$$

3. ALGEBRAIC DECAY OF SOLUTIONS AT LARGE DISTANCES

Following Wang [38], we investigate the asymptotic behavior of the solutions at large distances. Using the infinity boundary condition Eq. (22), for large ζ let

$$f \sim m + \theta(\zeta), \quad (29)$$

where $m = f(\infty)$ is a constant, $\theta \ll 1$ and θ decays to zero as $\zeta \rightarrow \infty$. Equation (15) linearizes to

$$\zeta \theta''' + (1 + A \text{Re} m) \theta'' = 0. \quad (30)$$

The only decay solution to Eq. (30) is

$$\theta = m_1 \zeta^{1-A \text{Re} m}, \quad (31)$$

$$\text{provided } m > \frac{1}{A \text{Re}}. \quad (32)$$

For large ζ consider

$$h \sim \psi \text{ and } g \sim \chi, \quad (33)$$

where ψ and χ are small. Using Eq. (33), Eqs. (16)-(17) linearized to

$$\zeta \chi'' + (1 + A \text{Re} m) \chi' + B \text{Re} \psi = 0, \quad (34)$$

$$\zeta \psi'' + (1 + CD \text{Re} \text{Pr} m) \psi' = 0. \quad (35)$$

The only decay solution to Eq. (35) is

$$\psi = m_2 \zeta^{-CD \text{Re} \text{Pr} m}. \quad (36)$$

Using (36), the general solution of (34) becomes

$$\chi = m_3 \zeta^{-A \text{Re} m} + m_4 \zeta^{(1-CD \text{Re} \text{Pr} m)}, \quad (37)$$

provided

$$m > \frac{1}{CD \text{Re} \text{Pr}}, \quad (38)$$

$$m_4 = \frac{-B \text{Re} m_2}{(CD \text{Re} \text{Pr} m - 1)(CD \text{Re} \text{Pr} m - 1 - A \text{Re} m)} \quad (39)$$

From Eqs. (32) and (38) we see that a necessary condition for the existence of solutions is

$$m > \max \left[\frac{1}{A \text{Re}}, \frac{1}{CD \text{Re} \text{Pr}} \right]. \quad (40)$$

It should be noted that for $\phi = 0$ i.e. $A = C = D = 1$, Eq. (40) exactly matches with the condition derived by Wang [38] for a base fluid.

4. NUMERICAL SOLUTIONS

Due to the algebraic decay of the solutions at large distances the domain is too large for accurate numerical integration. Thus, we compress the domain by an exponential transform, i.e.,

$$\zeta = e^\eta. \quad (41)$$

Now substituting (41) into Eqs. (15)-(17) we obtain

$$f_{\eta\eta\eta} - 2f_{\eta\eta} + f_\eta + A \text{Re} \left[f (f_{\eta\eta} - f_\eta) - f_\eta^2 \right] = 0, \quad (42)$$

$$g_{\eta\eta} + A \text{Re} \left[f g_\eta - g f_\eta \right] = -B \text{Re} e^\eta h, \quad (43)$$

$$h_{\eta\eta} + (1 + CD \text{Re} \text{Pr} f) h_\eta = 0. \quad (44)$$

Again, substituting (41) into (22); the boundary conditions become

$$f(0) = 0, f_\eta(0) = 1, f_\eta(\infty) = 0, \quad (45a)$$

$$g(0) = 0, g(\infty) = 0, \quad (45b)$$

$$h(0) = 1, \quad h(\infty) = 0. \quad (45c)$$

With the transformation (41), the skin-friction coefficient (24), the point of zero shear stress (25), and the Nusselt number (28) become

$$C_f = \frac{1}{(1-\phi)^{2.5}} \left[\frac{4\xi}{\text{Re}} \{f_{\eta\eta}(0) - f_\eta(0)\} + \frac{\gamma}{4\text{Re}} g_\eta(0) \right], \quad (46)$$

$$\xi = \frac{\gamma}{16} \left[\frac{g_\eta(0)}{f_\eta(0) - f_{\eta\eta}(0)} \right], \quad (47)$$

$$\text{Nu} = -\frac{2}{D} h_\eta(0). \quad (48)$$

The set of Eqs. (42)-(44) are highly nonlinear and coupled and cannot be solved analytically. The nonlinear system consisting of Eqs. (42)-(44) with boundary conditions (45) forms a two point boundary value problem (BVP) which are solved using the routine `bvp4c` available in the symbolic computer algebra software MATLAB after converting them into initial value problems (IVP). In applying this approach, we have to choose a finite value of the boundary $\eta \rightarrow \infty$, say η_{finite} . Care was exercised in choosing a suitable value of η_{finite} for a given set of parameters, typically $\eta \approx 2$ for large Re and $\eta \approx 8$ for small Re . Thus if the original independent variable ζ is used, "infinity" would range from e^2 to e^8 .

We construct the following first order differential equations

$$f_\eta = p_1, \quad p_1' = p_2$$

$$p_2' = 2p_2 - p_1 - A\text{Re} \left[f(p_2 - p_1) - p_1^2 \right], \quad (49)$$

$$g_\eta = p_3, \quad p_3' = -A\text{Re} \left[fp_3 - gp_1 \right] - B\text{Re} e^\eta h, \quad (50)$$

$$h_\eta = p_4, \quad p_4' = -(1 + CD\text{Re}Pr f)p_4, \quad (51)$$

with the initial conditions

$$f(0) = 0, \quad p_1(0) = 1, \quad g(0) = 0, \quad h(0) = 1. \quad (52)$$

To solve Eqs. (49)-(51) as an IVP we need values of $p_2(0) = f_{\eta\eta}(0)$, $p_3(0) = g_\eta(0)$ and $p_4(0) = h_\eta(0)$. From these equations we see that no such values are given. In the MATLAB routine `bvp4c` we need to guess initial values of $f_{\eta\eta}(0)$, $g_\eta(0)$, and $h_\eta(0)$ to obtain the solutions of (49)-(51) satisfying the initial conditions (52).

Because `bvp4c` uses a collocation formula, the numerical solution is based on a mesh of points at which the collocation equations are satisfied. Mesh selection and error control are based on the residual of this solution, such that the computed solution $S(x)$ is the exact solution of a perturbed problem $S'(x) = f(x, S(x)) + res(x)$. On each subinterval of the mesh, a norm of the residual in the i th component of the solution, $res(i)$, is estimated and is required to be less than or equal to a tolerance. This tolerance is a function of the relative and absolute tolerances, $RelTol$ and $AbsTol$, defined by

$$\|res(i) / \max(abs(f(i), AbsTol(i) / RelTol))\| \leq RelTol.$$

The convergence criterion is set to be 10^{-6} in all cases.

To test and assess grid independence of the present solution scheme, we ran the code with 100, 200 and 300 mesh points between $\eta = 0$ to $\eta = \eta_\infty$. In Table 3 we have calculated Nu using Eq. (48) for different values of Re using different mesh points. Table 3 reveals that 200 mesh points are adequate to describe correctly the heat transfer process over a stretching cylinder.

Table 3 Values of Nu for a base fluid ($\phi = 0$) for different values of Re and mesh points.

Re	Number of mesh points		
	100	200	300
2	3.347144 7	3.3471438	3.3471437
5	4.798543 7	4.7985336	4.7985339
10	6.436587 3	6.4364987	6.4364986
20	8.754535 9	8.7545954	8.7545957

To validate the present code we reproduced the values of $f_{\eta\eta}(0)$, $g_\eta(0)$ and $h_\eta(0)$ for different values of Pr and Re when $\phi = 0$. Tables 4(a)-(c) show that the values produced by the present code and those reported by Wang [38]. It is very important to note that *there is an error* in Eq. (33) of Wang [38]. The correct form of this equation is $h_{\eta\eta} + (1 + \text{Re}Pr f)h_\eta = 0$ and not $h_{\eta\eta} + \text{Re}Pr fh_\eta = 0$. The differences between the present and Wang [38] results in Tables 4(a)-(c) are due to this error. We are confident that results of Wang [38] can only be obtained by correcting the error in his paper. The present code produced $m = f(\infty) = 1.8740$ for $\text{Re} = 1$ and $m = f(\infty) = 0.3818$ for $\text{Re} = 10$ whereas the corresponding values produced by Wang [38] are 1.8786 and 0.3858 respectively. These values are in good agreement and confirm the validity of the present code.

Table 4(a) Comparison of the values of $f_{\eta\eta}(0)$ for $\phi = 0$.

Re	Pr	$f_{\eta\eta}(0)$	
		Present	Wang [38]
10	0.7	-2.3447	-2.3444
10	2.0	-2.3447	-2.3444
10	7.0	-2.3447	-2.3444
10	20	-2.3447	-2.3444
1	0.7	-0.1778	-0.1775
1	2.0	-0.1778	-0.1775
1	7.0	-0.1778	-0.1775
1	20	-0.1778	-0.1775

Table 4(b) Comparison of the values of $g_\eta(0)$ for $\phi = 0$.

Re	Pr	$g_\eta(0)$	
		Present	Wang [38]
10	0.7	2.6135	3.7270
10	2.0	1.5643	1.7808
10	7.0	0.8679	0.9210
10	20	0.5295	0.5474
1	0.7	0.6759	2.0629
1	2.0	0.4398	0.6415
1	7.0	0.2584	0.3087
1	20	0.1616	0.1791

Table 4(c) Comparison of the values of $h_\eta(0)$ for $\phi = 0$.

Re	Pr	$h_\eta(0)$	
		Present	Wang [38]
10	0.7	-2.3355	-1.568047
10	2.0	-3.7419	-3.035960
10	7.0	-6.8283	-6.157997
10	20	-11.4301	-10.77418
1	0.7	-1.3671	-0.58793
1	2.0	-1.7870	-1.06431
1	7.0	-2.7414	-2.05885
1	20	-4.1857	-3.52191

5. NUMERICAL RESULTS AND DISCUSSION

5.1 Heat transfer results

5.1.1 Effects of nanoparticle volume concentration and Reynolds number on the temperature distribution

The numerical calculations of nondimensional temperature as a function of η are shown in Figs. 2-3. In these calculations the values of the parameters, namely the nanoparticle volume concentration parameter ϕ , and the Reynolds number Re are varied keeping the Prandtl number Pr fixed. The simulations have been carried out for water based nanofluids containing Al_2O_3 , TiO_2 and Cu nanoparticles with 0-10% solid volume concentration. The value of the Prandtl number for the base fluid (water) was fixed at $Pr = 6.2$ (value at room temperature). The default values of other parameters are indicated in the description of the figures.

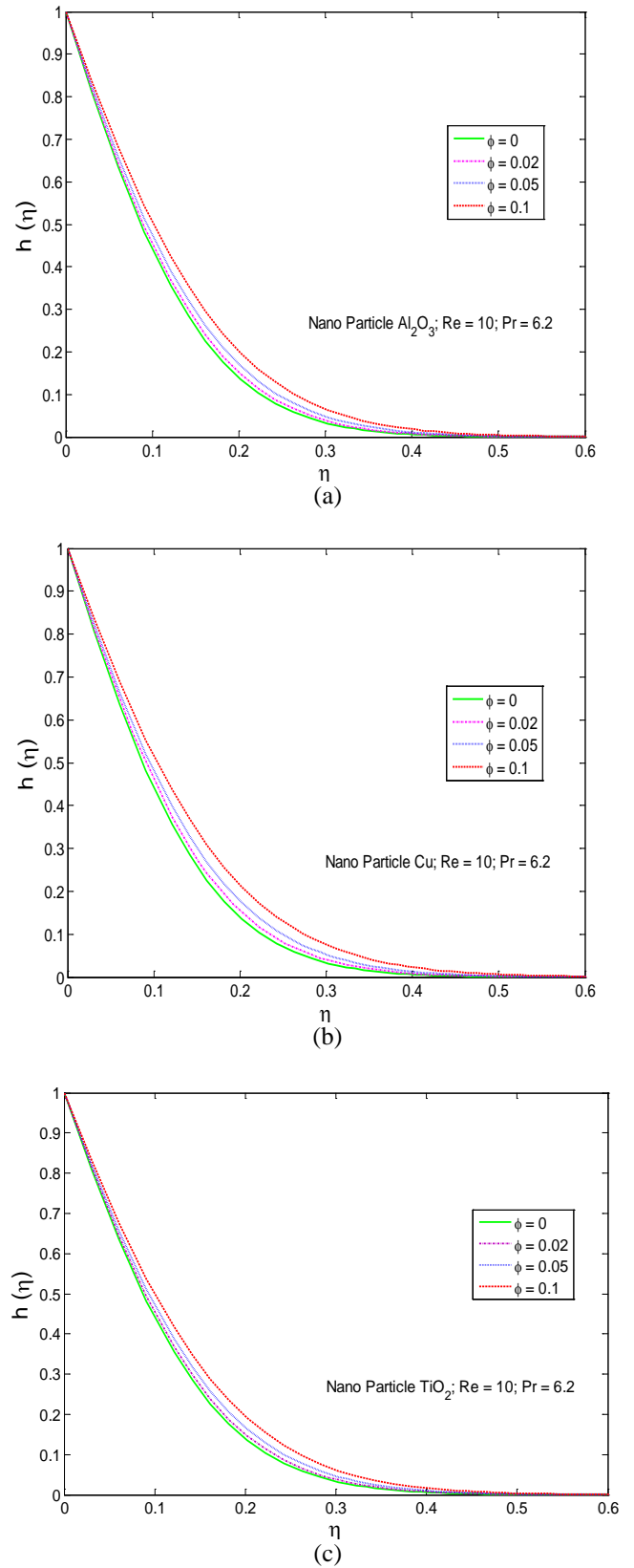


Figure 2 Temperature profiles for (a) Al_2O_3 - H_2O , (b) Cu - H_2O , and (c) TiO_2 - H_2O nanofluids for different values of ϕ and $Re = 10$.

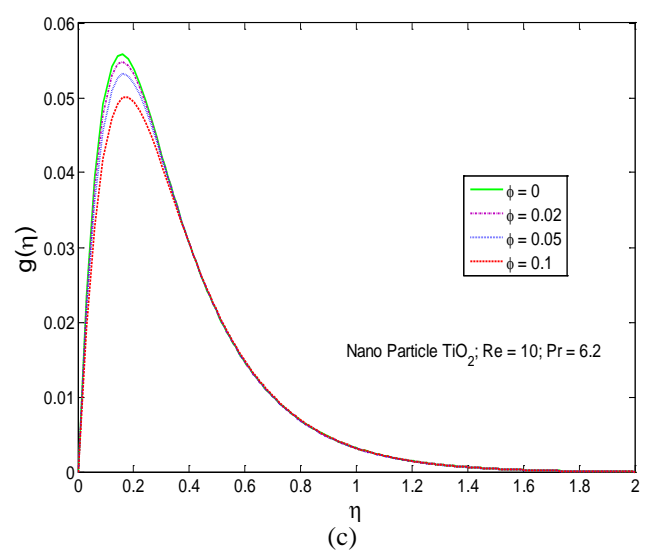
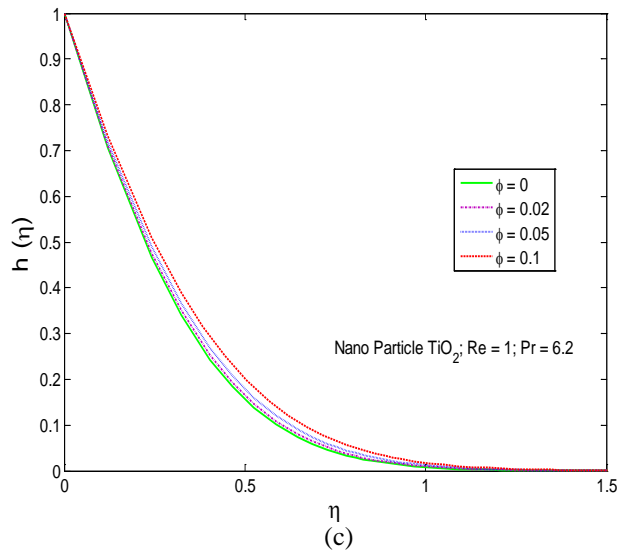
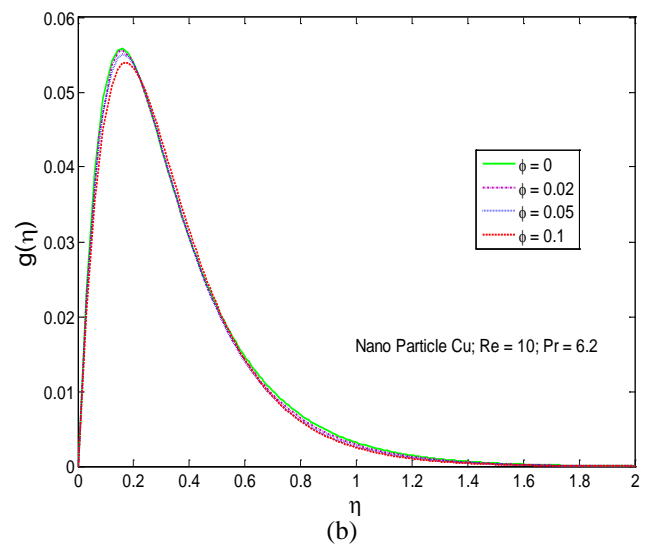
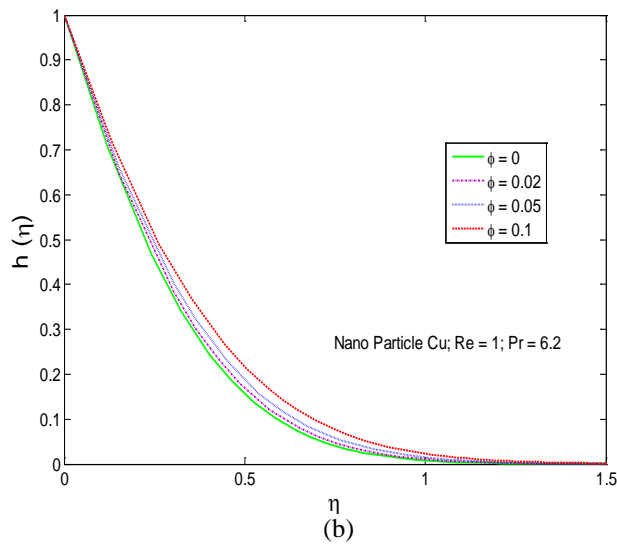
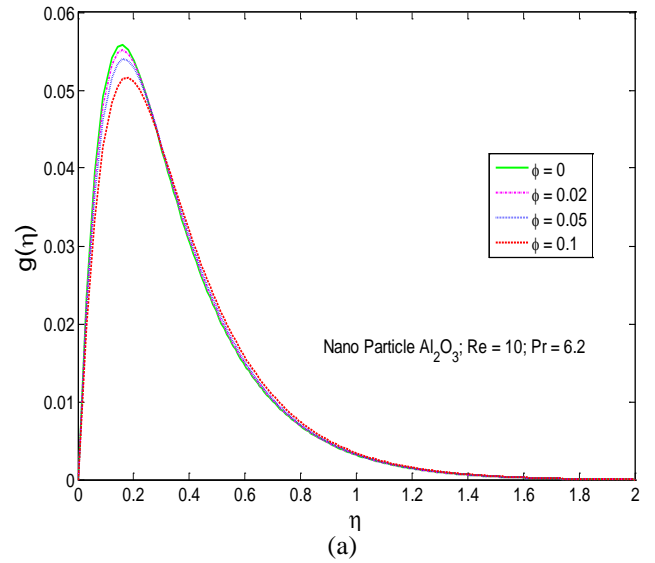
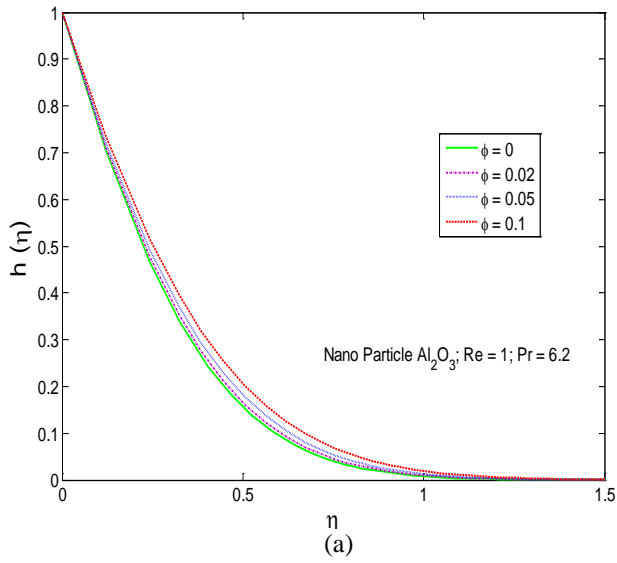


Figure 3 Temperature profiles for (a) $\text{Al}_2\text{O}_3\text{-H}_2\text{O}$, (b) $\text{Cu-H}_2\text{O}$, and (c) $\text{TiO}_2\text{-H}_2\text{O}$ nanofluids for different values of ϕ and $\text{Re} = 1$.

Figure 4 Axial velocity (g) profiles due to natural convection for (a) $\text{Al}_2\text{O}_3\text{-H}_2\text{O}$, (b) $\text{Cu-H}_2\text{O}$, and (c) $\text{TiO}_2\text{-H}_2\text{O}$ nanofluids for different values of ϕ and $\text{Re} = 10$.

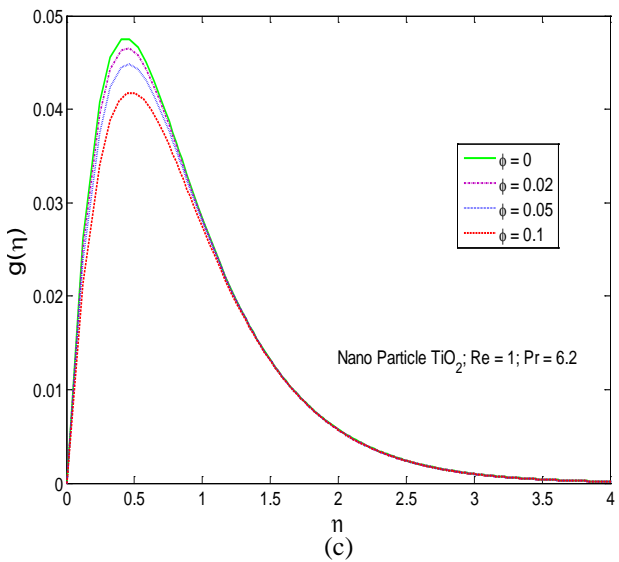
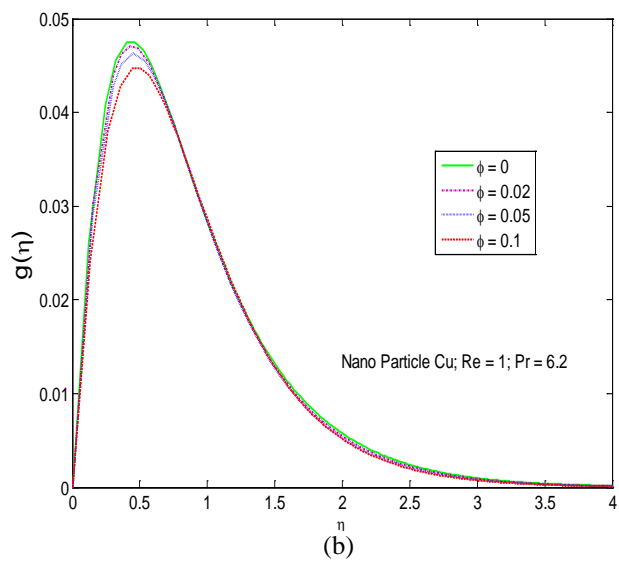
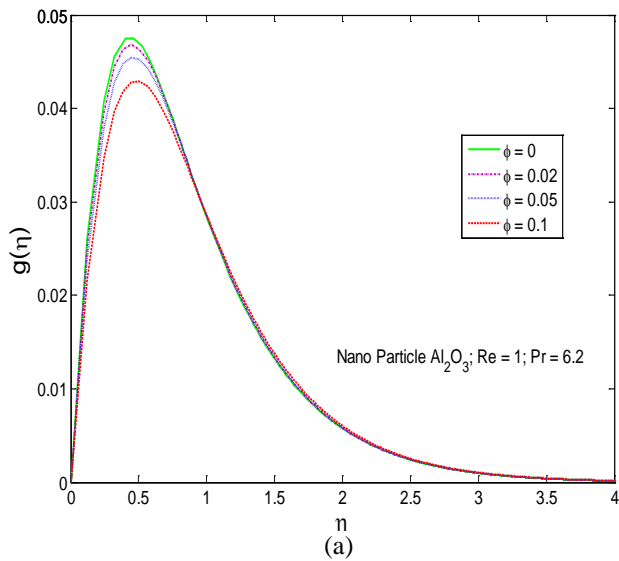


Figure 5 Axial velocity (g) profiles due to natural convection for (a) $\text{Al}_2\text{O}_3\text{-H}_2\text{O}$, (b) $\text{Cu-H}_2\text{O}$, and (c) $\text{TiO}_2\text{-H}_2\text{O}$ nanofluids for different values of ϕ and $\text{Re} = 1$.

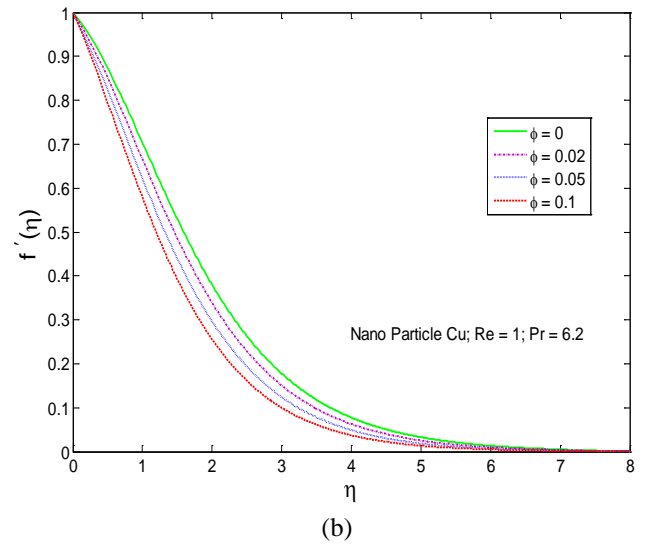
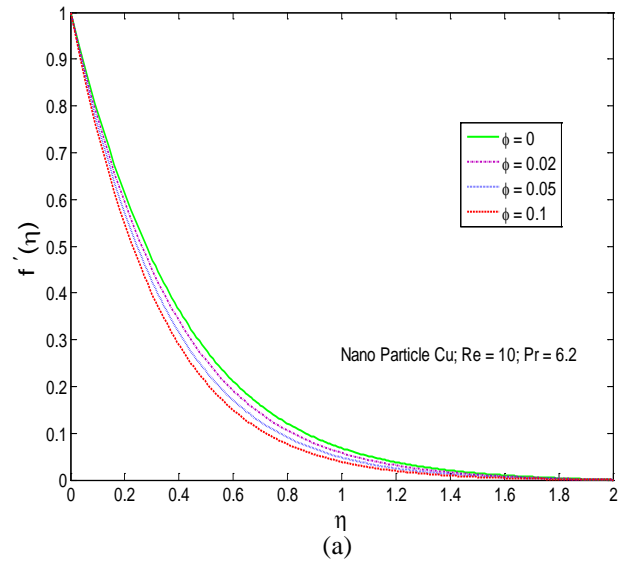
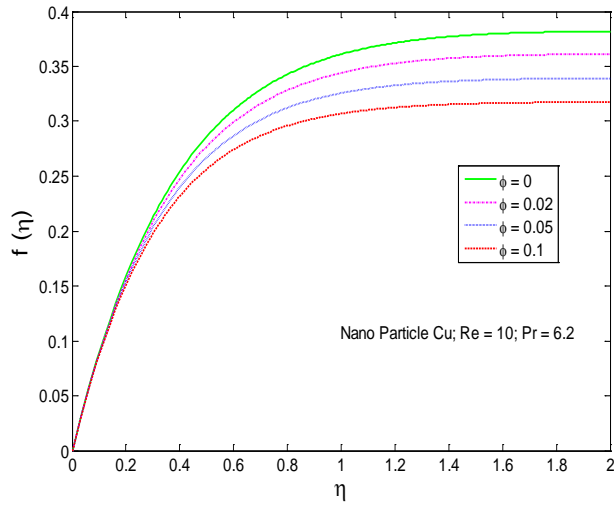
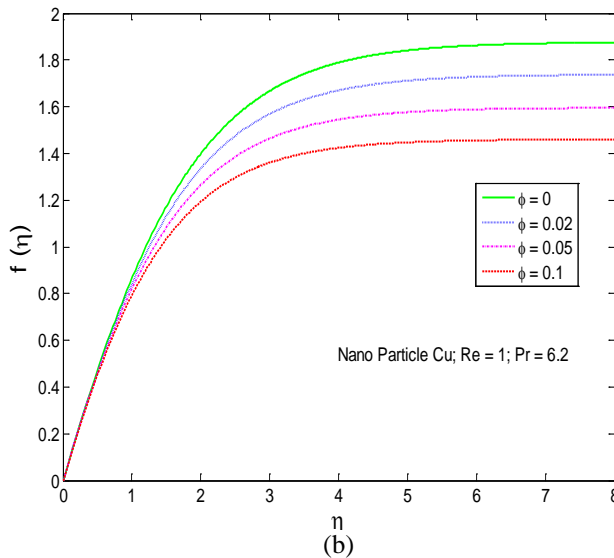


Figure 6 Axial velocity (f') profiles due to stretching for $\text{Cu-H}_2\text{O}$ nanofluid for different values of ϕ and (a) for $\text{Re} = 10$ and, (b) $\text{Re} = 1$.

Figures 2-3 illustrate the temperature profiles in the boundary layer for solid volume concentrations of $\phi = 0$ (0%), 0.02 (2%), 0.05 (5%), 0.1 (10%) for $\text{Re} = 10$ and $\text{Re} = 1$, respectively. These figures reveal that the local temperature in the boundary layer for different nanofluids increases (in general) with the increase in solid volume concentration of nanoparticles. It is also observed that the Cu-water nanofluid results in higher temperatures in the boundary layer compared with those produced in $\text{TiO}_2\text{-water}$ nanofluid. This difference in temperatures may be attributed to the higher thermal conductivity of Cu nanoparticles with that of TiO_2 nanoparticles. For both Cu-water and $\text{TiO}_2\text{-water}$ nanofluids, the local temperature in the boundary layer as well the thickness of the boundary layer increase as the solid volume fraction of the nanofluid increases.



(a)



(b)

Figure 7 Radial velocity (f) profiles for Cu-H₂O nanofluid for different values of ϕ and for (a) $Re = 10$ and, (b) $Re = 1$.

5.1.2 Effect of nanoparticle volume concentration on the Nusselt number

The rate of heat transfer in terms of Nusselt number for different values of the nanoparticles volume concentration (ϕ) is presented in Table 5. From the data we conclude that the rate of heat transfer increases significantly with the increase in the volume fraction of nanoparticles. On the other hand, for a given value of nanoparticles volume concentration (ϕ), one can observe that the heat transfer enhancement also becomes more important with the increase of the Reynolds number. These data further reveals that a better heat transfer can be achieved, compared to the base fluid, at lower Reynolds number for a fixed nanoparticles volume concentration. For example, with 5% solid volume concentration of TiO₂ nanoparticles, the Nusselt number increases about 7.2% compared with that of the base fluid (water) at Reynolds number of 1, and by 5.5% at Reynolds number of 10.

5.1.3 Comparison of Nusselt numbers for different nanofluids

In Table 5 we provide Nusselt number data for three water-based nanofluids. For a fixed solid volume concentration of nanoparticles, Cu-water nanofluid provides higher heat transfer rates compared with those realized with Al₂O₃-water and TiO₂-water nanofluids. As noted earlier, the explanation for higher heat transfer rate for Cu-water nanofluid lies in the fact that the thermal conductivity of Cu is relatively higher than Al₂O₃ and TiO₂.

Table 5 Values of Nu and ξ for different nanofluids and nanoparticles concentration levels.

Nano-particles	Re	ϕ	Nu	% change in Nu	$\xi\gamma^{-1}$
TiO ₂	1	0.00	5.2382	-----	0.0145
		0.02	5.3874	2.85	0.0137
		0.05	5.6176	7.24	0.0128
		0.10	6.0210	14.94	0.0113
	10	0.00	12.8728	-----	0.0171
		0.02	13.1534	2.18	0.0163
		0.05	13.5822	5.51	0.0152
		0.10	14.3226	11.26	0.0136
Al ₂ O ₃	1	0.00	5.2382	-----	0.0145
		0.02	5.4090	3.26	0.0138
		0.05	5.6762	8.36	0.0129
		0.10	6.1546	17.49	0.0116
	10	0.00	12.8728	-----	0.0171
		0.02	13.2142	2.65	0.0164
		0.05	13.7364	6.71	0.0154
		0.10	14.4460	12.22	0.0139
Cu	1	0.00	5.2382	-----	0.0145
		0.02	5.4164	3.40	0.0134
		0.05	5.6924	8.67	0.0122
		0.10	6.1794	17.97	0.0106
	10	0.00	12.8728	-----	0.0171
		0.02	13.1774	2.37	0.0159
		0.05	13.6496	6.03	0.0144
		0.10	14.4838	12.51	0.0126

5.2 Fluid flow results

5.2.1 Effects of nanoparticle volume concentration and Reynolds number on velocity distribution

We first consider the results for the component of the axial velocity g due to natural convection induced as a result of heating of the cylinder. Figures 4-5 present these results as a function of ϕ and Re . As the concentration of nanoparticles in the base fluid increases i.e. as ϕ increases, the peak value of the component g axial velocity decreases. As Re increases i.e. as the forced convection due to the stretching of the cylinder increases, the location of the peak value of g moves closer to the surface of the cylinder. This finding is consistent with the results of Wang [38] for a regular fluid. In other words, the essential feature of the fluid flow is not affected by the presence of nanoparticles.

Next in Fig. 6, we give the results for the component of the axial velocity due to forced convection induced as a result of the stretching of the cylinder, this component, represented by the function f' , decays more sharply as the nanoparticle concentration ϕ increases. The effect of Re on f' is more dramatic. For example, at $Re = 1$ (See Fig. 6b), the value of f' at $\eta = 1$ is much higher than the corresponding value at $Re = 10$ (See Fig. 6a). Again this observation corroborates the findings of Wang [38]. It is interesting to note that the axial velocity component f' (due to the forced convection of the stretching of the cylinder) dominates when the axial distance is small. On the other hand, the component of the axial velocity due to free convection g dominates when axial distance is large. Furthermore, the velocity of the fluid with nanoparticles is smaller than the velocity of the base fluid with no nanoparticles. The presence of the nanoparticles decreases the thickness of the hydrodynamic boundary layer.

Fig. 7 displays the radial component of the velocity for parametric values of the nanoparticle concentration and for $Re = 10$ and $Re = 1$. The radial velocity decreases as the concentration of nanoparticles increase. The radial velocity is higher for $Re = 1$ than for $Re = 10$.

5.2.2 Effect of nanoparticle volume concentration on shear stress

Equation (46) shows that the rate of shear stress depends on the axial distance ξ . The distances $\xi\gamma^{-1}$ at which C_f becomes zero for different parametric conditions are provided in Table 5. The data shows that the value of $\xi\gamma^{-1}$ given by Eq. (47) decreases with the increase in nanoparticle concentration for all three nanofluids. The point of zero shear stress occurs at larger axial distance as the Reynolds number increases.

6. CONCLUSIONS

In this paper, natural convection heat transfer in water based nanofluids over a stretching cylinder is studied numerically. Using similarity transformations, the mathematical equations describing the problem are transformed into nonlinear ordinary differential equations, and subsequently solved using MATLAB. Keeping in mind the algebraic decay of the similarity functions, numerical integration is performed using a compressed coordinate. The axial velocity is composed of forced convection due to stretching and natural convection induced by the heating of the cylinder. The present study has led to the following conclusions:

1. The velocity of the nanofluid is lower than the velocity of the base fluid with no nanoparticles.
2. The presence of nanoparticles tends to decrease the peak of the axial velocity due to natural convection.
3. The effect of the nanoparticles on the radial velocity is larger than its corresponding effect on the axial velocity.
4. With nanoparticles in the base fluid, the thickness of the hydrodynamic boundary layer is reduced.

5. With the addition of the nanoparticles the position of the zero shear stress on the surface of the cylinder is lowered.
6. The temperature of a nanofluid increases with the increase in nanoparticle concentration.
7. The thermal boundary layer is warmer for a nanofluid compared with that for a base fluid with no nanoparticles.
8. Addition of the nanoparticles to the base fluid enhances the rate of heat transfer from the stretching heated cylinder.
9. Better heat transfer can be achieved, compared to the base fluid, at lower Reynolds number for a fixed nanoparticles volume concentration.

Nomenclature

A	constant first appears in Eq. (15)
B	constant first appears in Eq. (16)
C	constant first appears in Eq. (17)
C_f	skin friction coefficient
c_p	specific heat at constant pressure (J/kg K)
D	constant first appears in Eq. (17)
f	dimensionless radial velocity
Gr_{bf}	local Grashof number
\tilde{g}	acceleration due to gravity (m/s ²)
g	dimensionless axial velocity due to natural convection
h	dimensionless temperature
k	constant appears in Eq. (13a)
m	constant appears in Eq. (29)
Nu	Nusselt number
Pr	Prandtl number
q_w	wall heat flux (W/m ²)
Re_{bf}	Reynolds number
T	local temperature of the nanofluid in the thermal boundary layer (K)
T_w	temperature at the surface of the cylinder (K)
T_∞	temperature of the ambient nanofluid (K)
u	radial velocity (m/s)
w	axial velocity (m/s)
r	distance along the radial direction (m)
z	distance along the axial direction (m)

Greek symbols

α_{nf}	effective thermal diffusivity of nanofluid (m ² /s)
α_{bf}	effective thermal diffusivity of base fluid (m ² /s)
β	volumetric coefficient of thermal expansion of nanofluid (1/K)
β_{bf}	volumetric coefficient of thermal expansion of base fluid (1/K)
γ	Richardson parameter
ρ_{nf}	effective density of the nanofluid (kg/m ³)
ρ_{bf}	density of the base fluid (kg/m ³)

$(\rho c)_{nf}$ effective heat capacity of the nanofluid (J/K)

$(\rho c)_{bf}$ heat capacity of the base fluid (J/K)

μ_{nf} effective dynamic viscosity of the nanofluid (Pa s)

μ_{bf} dynamic viscosity of the base fluid (Pa s)

ν_{nf} kinematic coefficient of viscosity of nanofluid (m^2/s)

ν_{bf} kinematic coefficient of viscosity of base fluid (m^2/s)

κ_{nf} thermal conductivity of nanofluid (W/m K)

κ_{bf} thermal conductivity of base fluid (W/m K)

χ same as g

ϕ solid volume fraction of nanofluid

ψ same as h

ζ similarity variable

η compressed similarity variable

ξ nondimensional axial distance

θ a function that appears first in Eq. (29)

Subscripts

w surface

nf nanofluid

bf base fluid

sp solid particle

∞ conditions far away from the surface

Superscripts

' differentiation with respect to ζ

containing copper nanoparticles, Appl. Phys. Lett. Vol. 78, pp. 718-720, 2001.

- [9] S.M.S. Murshed, K.C. Leong, and C. Yang, Enhanced thermal conductivity of TiO_2 -water based nanofluids, Int. J. Thermal Sci. Vol. 44, pp. 367-373, 2005.
- [10] K. Khanafer, K. Vafai, and M. Lightstone, Buoyancy-driven heat transfer enhancement in a two-dimensional enclosure utilizing nanofluids, Int. J. Heat Mass Transf. Vol. 46, pp. 3639-3653, 2003.
- [11] S.E.B. Maiga, S.J. Palm, C.T. Nguyen, G. Roy, and N. Galanis, Heat transfer enhancement by using nanofluids in forced convection flows, Int. J. Heat Fluid Flow Vol. 26, pp. 530-546, 2005.
- [12] R.Y. Jou, and S.-C. Tzeng, Numerical research of nature convective heat transfer enhancement filled with nanofluids in rectangular enclosures, Int. Commu. Heat Mass Transf. Vol. 33, pp.727-736, 2006.
- [13] K.S. Hang, Ji-H. Lee, and S.P. Jang, Buoyancy-driven heat transfer of water-based nanofluids in a rectangular cavity, Int. J. Heat Mass Transf. Vol. 50, pp. 4003-4010, 2007.
- [14] R.K. Tiwari, and M.K. Das, Heat transfer augmentation in a two-sided lid-driven differentially heated square cavity utilizing nanofluids. Int. J. Heat Mass Transf. Vol. 50, pp. 2002-2018, 2007.
- [15] H.F. Oztop, and E. Abu-Nada, Numerical study of natural convection in partially heated rectangular enclosures filled with nanofluids, Int. J. Heat Fluid Flow Vol. 29, pp. 1326-1336, 2008.
- [16] E. Abu-Nada, and H.F. Oztop, Effects of inclination angle on natural convection in enclosures filled with Cu-water nanofluid, Int. J. Heat Fluid Flow. Vol. 30, pp. 669-678, 2009.
- [17] M. Muthtamilselvan, P. Kandaswamy, and J. Lee, Heat transfer enhancement of copper-water nanofluids in a lid-driven enclosure, Commun. Nonlinear Sci. Numer. Simul. Vol. 15, pp. 1501-1510, 2010.
- [18] A.V. Kuznetsov, and D.A. Nield, Natural convective boundary-layer flow of a nanofluid past a vertical plate, Int. J. Thermal Sci. Vol. 49, pp. 243-247, 2010.
- [19] N. Bachok, A. Ishak, and I. Pop, Boundary-layer flow of nanofluids over a moving surface in a flowing fluid, Int. J. Thermal Sci. Vol. 49, pp. 1663-1668, 2010.
- [20] W.A. Khan, and A. Aziz, Natural convection flow of a nanofluid over a vertical plate with uniform surface heat flux, Int. J. Thermal Sci. Vol. 50, pp. 1207-1214, 2011.
- [21] A. Aziz, and W.A. Khan, Natural convective boundary layer flow of a nanofluid past a convectively heated vertical plate, Int. J. Thermal Sci. Vol. 52, pp. 83-90, 2012.
- [22] M.M. Rahman, M. A. Al-Lawatia, I.A. Eltayeb, and N. Al-Salti, Hydromagnetic slip flow of water based nanofluids past a wedge with convective surface in the presence of heat generation (or) absorption, Int. J. Thermal Sci. Vol. 57, pp. 172-182, 2012.
- [23] M.M. Rahman, and I.A. Eltayeb, Radiative heat transfer in a hydromagnetic nanofluid past a non-linear stretching surface with convective boundary condition, Meccanica. doi: 10.1007/s11012-012-9618-2.

References

- [1] S. Choi, Enhancing thermal conductivity of fluids with nanoparticle, in: D.A. Siginer, H.P. Wang (Eds.), Developments and Applications of Non-Newtonian Flows, ASME FED, vol. 231/MD-Vol. 66, pp. 99-105, 1995.
- [2] H. Masuda, A. Ebata, K. Teramae, and N. Hishinuma, Alteration of thermal conductivity and viscosity of liquid by dispersing ultra-fine particles. Netsu. Bussei. Vol. 7, pp. 227-233, 1993.
- [3] S. Lee, S.U.S. Choi, S. Li, and J.A. Eastman, Measuring thermal conductivity of fluids containing oxide nanoparticles, J. Heat Transf. Vol. 121, pp. 280-289, 1999.
- [4] Y. Xuan, and Q. Li, Heat transfer enhancement of nanofluids, Int. J. Heat Fluid Transf. Vol. 21, pp. 58-64, 2000.
- [5] Y. Xuan, and W. Roetzel, Conceptions for heat transfer correlation of nanofluids, Int. J. Heat Mass Transf. Vol. 43, pp. 3701-3707, 2000.
- [6] J. Buongiorno, Convective transport in nanofluids. ASME J. Heat Transf. Vol. 128, pp. 240-250, 2006.
- [7] C. Kleinstreuer, J. Li, and J. Koo, Microfluidics of nano-drug delivery. Int. J. Heat Mass Transf. Vol. 51, pp. 5590-5597, 2008.
- [8] J.A. Eastman, S.U.S. Choi, S. Li, W. Yu, and L.J. Thompson, Anomalously increased effective thermal conductivities of ethylene glycol based nanofluids

- [24] S. Kakaç, and A. Pramuanjaroenkij, Review of convective heat transfer enhancement with nanofluids. *Int. J. Heat Mass Transf.* Vol. 52, pp. 3187–3196, 2009.
- [25] S.K. Das, S.U.S. Choi, W. Yu, and T. Pradeep, *Nanofluids: Science and Technology*. Wiley, New Jersey, 2007.
- [26] V. Trisaksri, and S. Wongwises, Critical review of heat transfer characteristics of nanofluids. *Renew. Sustain. Energy Rev.* Vol. 11, pp. 512-523, 2007.
- [27] X.Q. Wang, and A.S. Mujumdar, A review on nanofluids—Part I: theoretical and numerical investigations, *Braz. J. Chem. Eng.* Vol. 25, pp. 613–630, 2008.
- [28] X.Q. Wang, and A.S. Mujumdar, A review on nanofluids—Part II: experiments and applications, *Braz. J. Chem. Eng.* Vol. 25, pp. 631–648, 2008.
- [29] L.J. Crane, Flow Past a Stretching Plate, *Z. Angew Math. Phys.* Vol. 21, pp. 645–647, 1970.
- [30] C.Y. Wang, The three-dimensional flow due to a stretching flat surface, *Phys. Fluids* Vol. 27, pp. 1915-1917, 1984.
- [31] H.I. Andersson, K.H. Bech, and B.S. Dantapat, Magnetohydrodynamic flow of a power-law fluid over a stretching sheet, *Int. J. Nonlinear Mech.* Vol. 27, pp. 929–936, 1992.
- [32] E.M.A. Elbashbeshy, Heat transfer over a stretching surface with variable surface heat flux, *J. Phys. D: Appl. Phys.* Vol. 31, pp. 1951–1954, 1998.
- [33] M.M. Rahman, and M.A. Al-Lawatia, Effects of higher order chemical reaction on micropolar fluid flow on a power law permeable stretched sheet with variable concentration in a porous medium, *Can. J. Chem. Eng.* Vol. 88, pp. 23–32, 2010.
- [34] M.M. Rahman, Combined effects of internal heat generation and higher order chemical reaction on the non-Darcian forced convective flow of a viscous incompressible fluid with variable viscosity and thermal conductivity over a stretching surface embedded in a porous medium, *Can. J. Chem. Eng.* doi: 10.1002/cjce.20644.
- [35] J.F. Brady, and A. Acrivos, Steady flow in a channel or tube with an accelerating surface velocity, *J. Fluid Mech.* Vol. 112, pp. 127-150, 1981.
- [36] C.Y. Wang, Fluid flow due to a stretching cylinder, *Phys. Fluids* Vol. 31, pp. 466-468, 1988.
- [37] A. Ishak, R. Nazar, and I. Pop, Uniform suction/blowing effect on flow and heat transfer due to a stretching cylinder, *App. Math. Modeling* Vol. 2, pp. 2059-2066, 2008.
- [38] C.Y. Wang, Natural convection on a vertical stretching cylinder, *Commu. Nonlin. Sci. Numer. Simulat.* Vol. 17, pp. 1098-1103, 2012.
- [39] W.A. Khan, and I. Pop, Boundary-layer flow of a nanofluid past a stretching sheet, *Int. J. Heat Mass Transf.* Vol. 53, pp. 2477–2483, 2010.
- [40] A.A.A. Hamad, and I. Pop, Scaling transformations for boundary layer flow near the stagnation-point on a heated permeable stretching surface in a porous medium saturated with a nanofluid and heat generation/absorption effects, *Transp. Porous Med.* Vol. 87, pp. 25–39, 2011.
- [41] S.M. Sebdani, M. Mahmoodi, and S.M. Hashemi. Effect of nanofluid variable properties on mixed convection in a square cavity, *Int. J. Thermal Sci.* Vol. 52, pp. 112-126, 2012.
- [42] A.V. Kuznetsov, and D.A. Nield, Double-diffusive natural convective boundary-layer flow of a nanofluid past a vertical plate, *Int. J. Thermal Sci.* Vol. 50, pp. 712-717, 2011.
- [43] D.A. Nield, and A.V. Kuznetsov, The Cheng–Minkowycz problem for the double-diffusive natural convective boundary layer flow in a porous medium saturated by a nanofluid, *Int. J. Heat Mas Transf.* Vol. 54, pp. 374-378, 2011.
- [44] K.P. Travis, B.D. Todd, and D.J. Evans. Poiseuille flow of molecular liquids, *Physica A* Vol. 240, pp. 315-327, 1997.
- [45] B. Straughan. Green-Naghdi fluid with non-thermal equilibrium effects, *Proc. Roy. Soc. London A* Vol. 466, pp. 2021-2032, 2010.
- [46] H.C. Brinkman, The viscosity of concentrated suspensions and solutions, *J. Chem. Phys.* Vol. 20, pp. 571–581, 1952.
- [47] Y. Xuan, and Q. Li, Investigation on convective heat transfer and flow features of nanofluids, *ASME J. Heat Transf.* Vol. 125, pp. 151–155, 2003.
- [48] M.A. Mansour, and S.E. Ahmed, Mixed convection flows in a square lid-driven cavity with heat source at the bottom utilizing nanofluid, *The Canadian J. Chem. Eng.*, doi: 10.1002/cjce.20533.
- [49] R.L. Hamilton, and O.K. Crossner, Thermal conductivity of heterogeneous two-component system, I and EC Fundamentals, Vol. 1, pp. 187-191, 1962.
- [50] C.J. Ho, M.W. Chen, and Z.W. Li, Numerical simulation of natural convection of nanofluid in a square enclosure: effects due to uncertainties of viscosity and thermal conductivity, *Int. J. Heat Mass Transf.* Vol. 51, pp. 4506–4516, 2008.
- [51] M.K. Das, and P.S. Ohal, Natural convection heat transfer augmentation in a partially heated and partially cooled square cavity utilizing nanofluids, *Int. J. Numer. Meth. Heat Fluid Flow* Vol. 19, pp. 411-431, 2009.